Electronic Supplementary Material (ESI) for Chemical Science.

Supporting Information for

Janus interface enables reversible Zn-ion battery by regulating interfacial water structure and crystal-orientation

Yuxuan Liang†, Meijia Qiu†, Peng Sun, and Wenjie Mai**

Siyuan Laboratory, Guangzhou Key Laboratory of Vacuum Coating Technologies and New Energy Materials, Guangdong Key Laboratory of Optical Fiber Sensing and Communications, Guangdong Provincial Key Laboratory of Nanophotonic Manipulation, Guangdong Provincial Engineering Technology Research Center of Vacuum Coating Technologies and New Energy Materials, Department of Physics, Jinan University, Guangdong 510632, People's Republic of China.

Email: sunp0421@jnu.edu.cn (P. Sun); wenjiemai@email.jnu.edu.cn (W. Mai)

Experimental Methods

Preparation of MnO_2 electrode

MnO_2 electrodes were fabricated on carbon cloth by the electroplating method. Before the depositing process, the carbon cloth was first washed step by step with acetone, ethanol, and deionized water under an ultrasonic bath each for 10 mins. The MnO_2 electrode was prepared using 0.1 M $MnAc_2$ and 0.1 M Na_2SO_4 solution as the plating solution in a three-electrode system with Ag/AgCl as the reference electrode, C as the counter electrode. The plating conditions were set to be 4 mA cm^{-2} for 10 min. The deposited MnO_2 was then washed by DI water and dried at 60 °C for over 6 h.

Fabrication of Zn//Zn cells, Zn//Cu cells and Zn-MnO_2 full cell

Commercial Zn sheets with different thickness (100 μm/20 μm) with a clean surface were used as two electrodes for the Zn//Zn cell. 75 μL of 1 M $Zn(ClO_4)_2$ electrolyte and 1 M $Zn(ClO_4)_2$ containing different concentrations of MET were added to the coin cell, respectively, and a piece of glass fiber (GE-Whatman, 125 μm) was used to separate the two electrodes. For the Zn//Cu cell, one of the Zn sheets in the Zn//Zn cell was replaced by a Cu sheet (100 μm), while For the Zn-MnO_2 full cell, one of Zn sheets in the Zn//Zn cell was replaced with a MnO_2 as the cathode, and other conditions were kept constant.

Electrochemical Test

The performance of Zn//Zn cells, Zn//Cu cells, and Zn-MnO_2 full cells were collected by a Neware battery test system (CT-4008Tn-5V10mA-164, Shenzhen, China). For the Zn//Zn cell, constant current densities ranging from 1, 5, and 10 mA cm^{-2} were applied, and both charging and discharging times were set to 1 hour. For the 30% DOD test of Zn//Zn cells, the charge/discharge rate is 1C and the Zn anode was replaced by a thicker Zn foil 20 μm. For Zn//Cu cells, the current density is 1 mA cm^{-2} and both charging and discharging times are set to 0.5 hours. For Zn-MnO_2 cells, cyclic measurements were performed at different current densities (0.1 to 1A g^{-1}) with a voltage range of 1-1.9 V. The

nucleation overpotential test was applied at a current density of 1 mA cm^{-2} and a discharge time of 24 h. The electrochemical performances of the Zn foil anode were all performed in an electrochemical workstation (CHI 760e) using a three-electrode system (Zn foil as the working electrode, Pt as the counter electrode, and Ag/AgCl as the reference electrode). For cyclic voltammetry (CV) tests, the voltage range was -0.2 V to -1.3 V with a scan rate of 1 mV s^{-1}. For the chronoamperometry curve, the initial voltage was -1.09 V and the set-up time was 10 min. Hydrogen evolution properties were collected by linear voltammetry scanning (LSV) with a potential range of -0.9 to -1.6 V at the scan rate of 1 mV s^{-1}. The Tafel tests representing the corrosion performance were conducted within the potential window ranging from -0.6 to -1.2 V at a scan rate of 1 mV s^{-1}. For electrochemical impedance spectra, Zn-Zn symmetric cells with different electrolytes were tested at frequencies ranging from 0.1 Hz to 100 kHz and temperatures ranging from 30 °C to 80 °C. The activation energy was calculated by the Arrhenius equation:

$$\frac{1}{R_{ct}} = Aexp(-\frac{E_\alpha}{RT}) \quad (1)$$

where R_{ct} is the electrochemical impedance, R is the molar gas constant, T is thermodynamic temperature, E_α is the activation energy, and A is the frequency factor. For the differential capacitance curve, it is collected by Impedance-Potential test with a voltage range of -1.5 V to 0.5 V and a scan rate of 10 mV s^{-1}. The differential capacitance is calculated as

$$C_d = \frac{1}{2\pi f Z_{im}} \quad (2)$$

Where C_d is the differential capacitance, f is the frequency, Z_{im} is the imaginary part of the impedance.

Characterization

The in-situ microscope images for Zn deposition process were obtained by a commercial high-resolution camera (Mshot, MS60) equipped the magnifying glass holder. The morphology of Zn foil before and after deposition or cycles was characterized by field-

emission scanning electron microscopy (SEM, ZEISS ULTRA 55). The crystal structure and material composition information were gathered by X-ray diffraction (XRD, Rigaku, MiniFlex600, Cu Kα/Xpert Pro mrd). Electrode surface elemental analysis was collected by X-ray photoelectron spectroscopy (XPS, Thermo Scientific™ K-Alpha™). Zeta potential was collected by a zeta potential analyzer (Austria, Anton Paar surpass).

Ab-initial calculations

The calculation of the interaction between Zn slab exposing different crystal surfaces and absorbed/desorbed atoms/molecules were all performed by the CP2K package.[1] PBE functional and Kohn-Sham DFT were used to describe the system and electronic structure in the framework of the Gaussian and plane waves method, respectively.[2] The Goedecker-Teter-Hutter (GTH) pseudopotentials and DZVP-MOLOPT-SR-GTH basis set were conducted for describing atoms in the system.[3, 4] A plane-wave energy cut-off and relative cut-off of 500 Ry and 60 Ry have been employed, respectively, while the energy convergence criterion was set to 10^{-6} Hartree.

Geometry optimization, single-point energy for Zn (002), (100), (101) were carried out within a 10.6596 × 10.6596 × 27.4202 $Å^3$, 10.6596 × 19.7872 × 23.0772 $Å^3$, 22.4758 × 10.6596 × 22.4400 $Å^3$ boxes under a periodic boundary condition with dense Monkhorst-Pack k point meshes of 2 × 2 × 1, 2 × 1 × 1, 1 × 2 × 1, respectively. On the Z direction, there is a 15 Å vacuum layer for avoiding the effect of periodic condition for slab model in z axis. A 4×4 supercell with four-layer Zn slab exposing different crystal planes was used to represent the absorbed/desorbed surface for atoms/molecules, and the bottom two layers were kept fixed to maintain the bulk property.

The absorbed energy between Zn slab and H_2O or MET molecules was defined as following equation:

$$E_{abs(m/a).} = E_{Zn\text{-}slab+m/a} - E_{Zn\text{-}slab} - E_{m/a}$$

and the absorbed and desorbed energy between Zn atom and Zn-MET were defined by following equations:

Absorbed energy: $E_{dbs.} = E_{Zn\text{-}MET + one\ Zn\ atom} - E_{Zn\text{-}slab} - E_{Zn\ atom}$

Desorbed energy: $E_{dbs.} = E_{Zn\text{-}MET - one\ Zn\ atom} - E_{Zn\text{-}slab} + E_{Zn\ atom}$

MD simulation

MD simulations were performed by the GROMACS software.[5, 6] Amber and GAFF force fields were employed. The size of box is 3.2 × 2.8 ×6.5 nm^3, with periodic boundary conditions in all three directions. The simulation system contains 1375 H_2O, 25 Zn^{2+},50 ClO_4^-, 10 MET and a Zn crystal. PME methods were utilized to compute the electrostatic interactions. A cutoff length of 1.0 nm was used in the calculation of electrostatic interactions and non-electrostatic interactions in real space and the integration time step was 1 fs. The temperature and pressure coupling were performed in V-rescale and Berendsen method, respectively. Finally, a 20-ns production simulation was conducted. The pressure coupling method in production simulation period was changed to Parrinello-Rahman.

Discussion S1

The pH values of 1 M $Zn(ClO_4)_2$ electrolyte and 1 M $Zn(ClO_4)_2$ + 50 mM MET electrolyte were measured to be 3.90 and 2.93, respectively (shown in Table S1), indicating that the addition of MET indeed led to a decrease in pH value. To verify whether the improved performance was caused by the decreased pH value, 1 M $Zn(ClO_4)_2$ + 0.248 mM $HClO_4$ electrolyte with a similar pH value (2.95) to the $Zn(ClO_4)_2$-MET electrolyte was prepared. By comparing the performance of Zn//Zn cells using the 1 M $Zn(ClO_4)_2$ and 1 M $Zn(ClO_4)_2$ + 0.248 mM $HClO_4$ electrolytes, it can be found that the decrease in pH value in the latter system could hardly bring improvement for the stability of Zn anodes. Therefore, the decreased pH value caused by the MET additive is not a critical factor affecting the performance of the cells (Fig. S16).

Figure captions

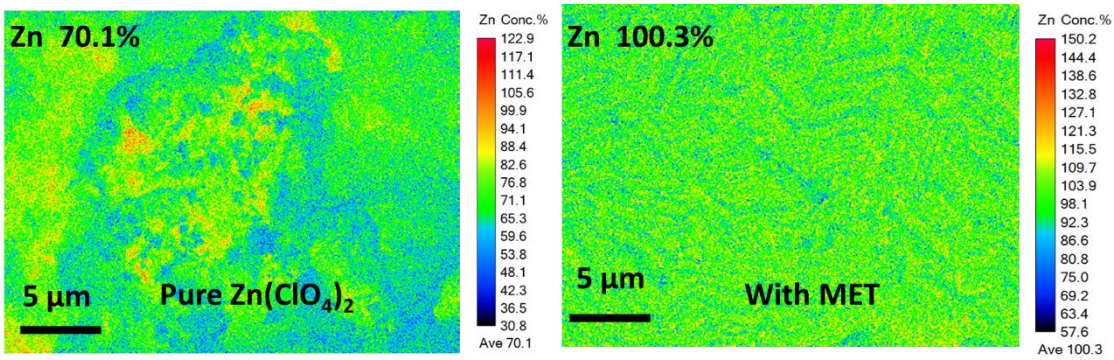

Fig. S1 Results of EPMA of the deposited Zn layer obtained in different electrolytes under the plating condition of 10 mA cm^{-2} for 1 h.

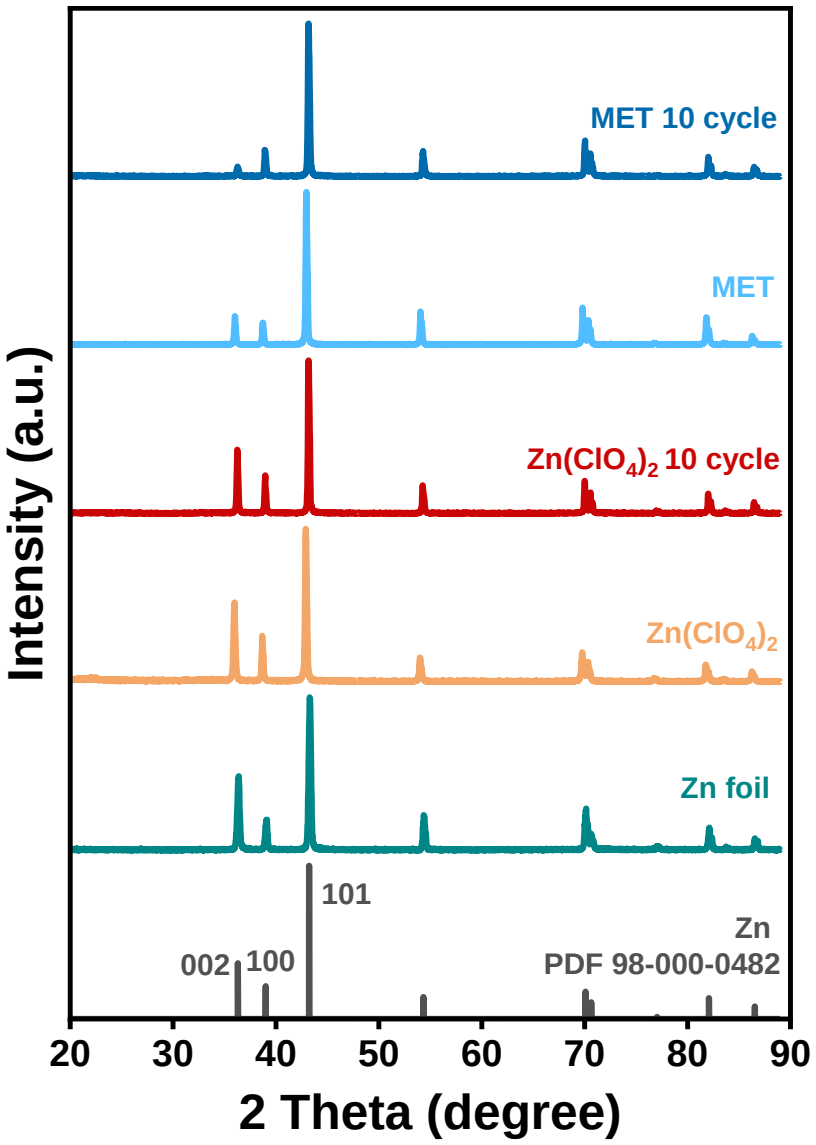

Fig. S2 2D figure of XRD patterns of Zn foil after several cycles in different electrolytes with 10 mA cm^{-2} and 10 mAh cm^{-2}.

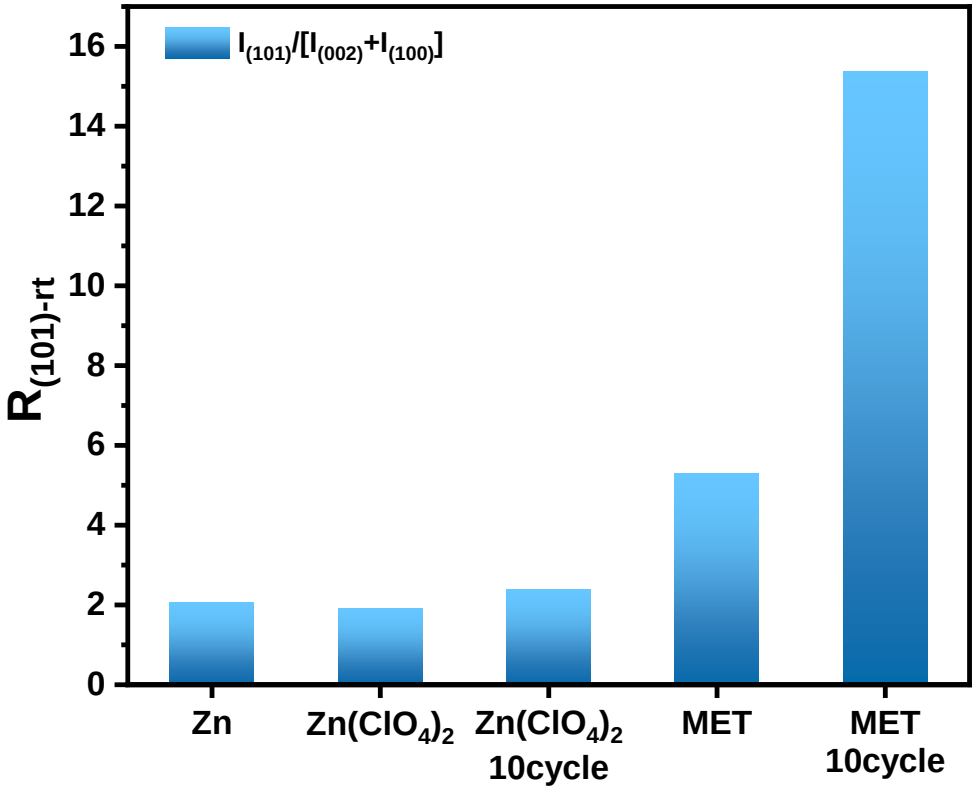

Fig. S3 Ratio of the intensity of Zn(101) to the sum of the intensities of Zn(002) plus Zn(100) in XRD.

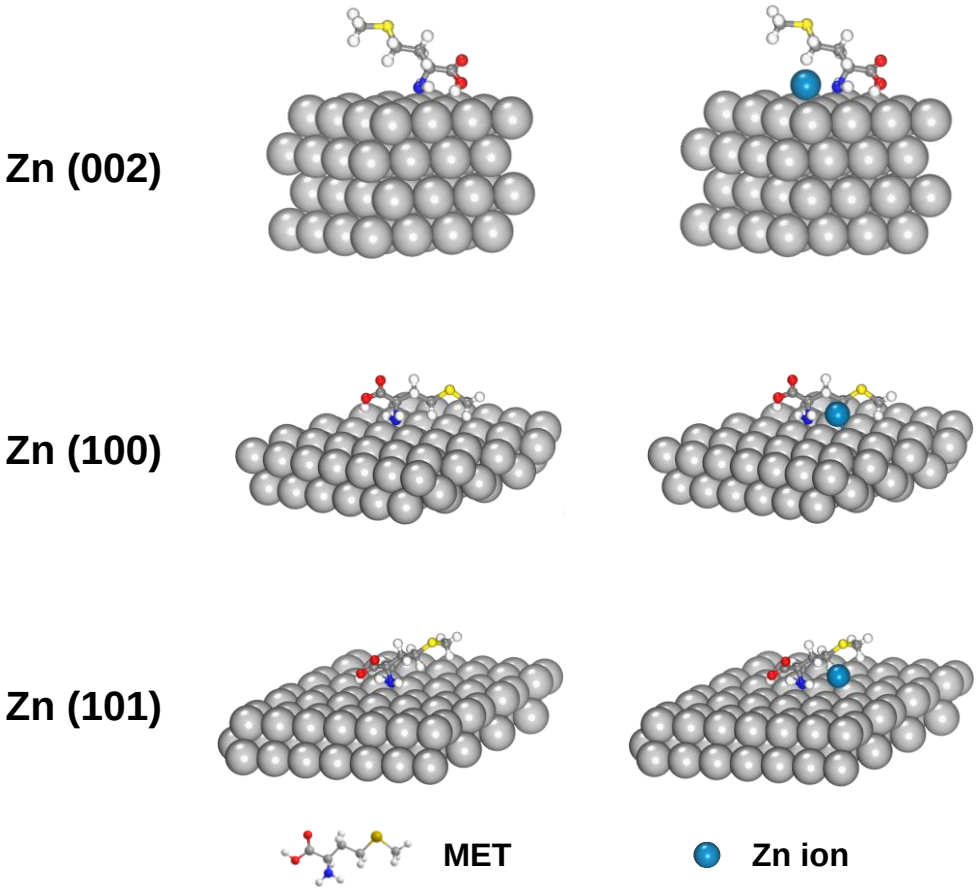

Fig. S4 DFT model of adsorption of MET molecules and Zn2+ on different crystal planes of the Zn anode.

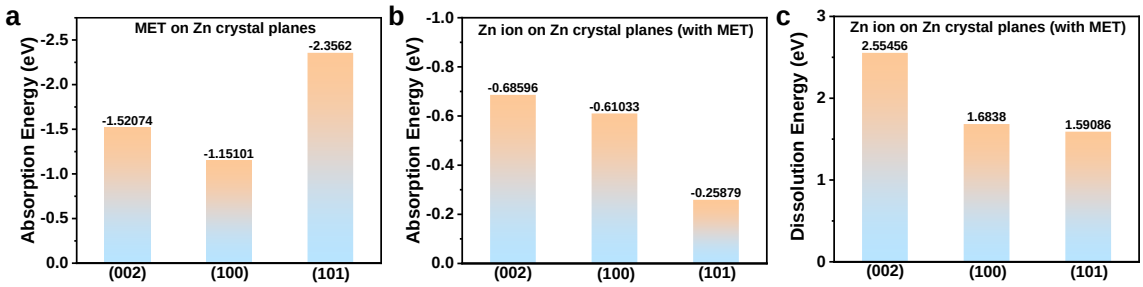

Fig. S5 (a) Adsorption energy of MET on different crystal plane surfaces of pure Zn anode; (b) Adsorption energy and (c) dissolution energy of Zn ion on different crystalline surfaces of Zn anode with absorbed MET.

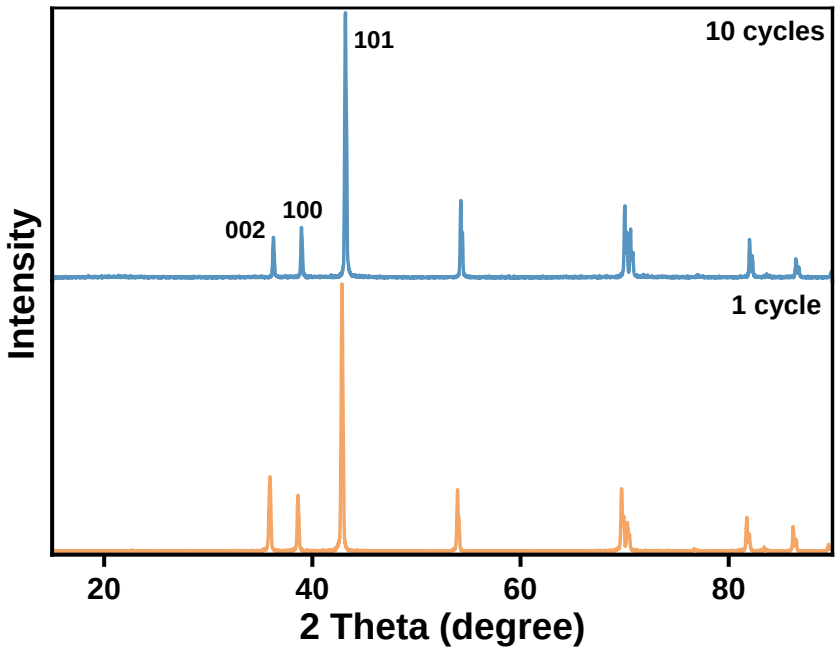

Fig. S6 XRD patterns of the Zn stripping surface at different cycle using the $Zn(ClO_4)_2$-MET electrolyte.

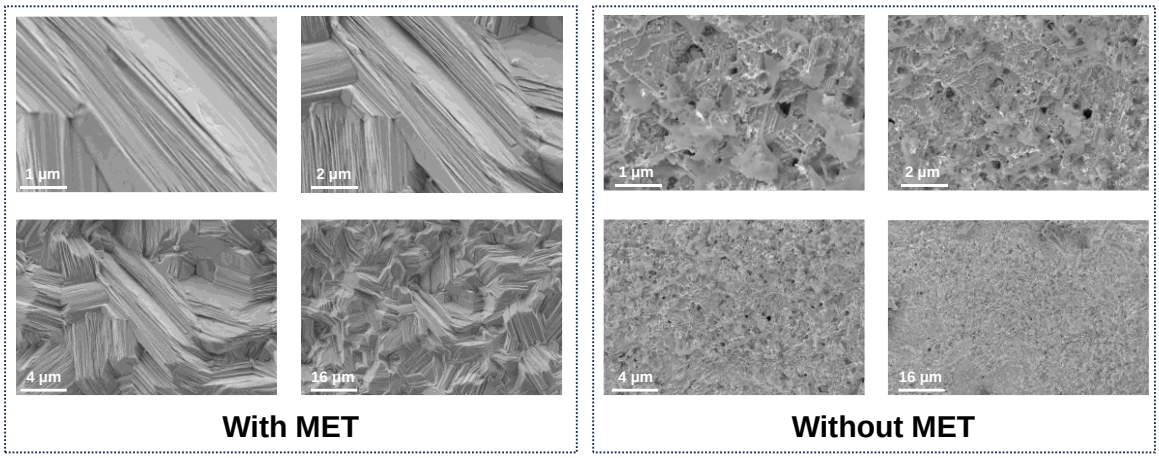

Fig. S7 SEM image of deposited surfaces of the Zn anode after 10 plating/stripping in $Zn(ClO_4)_2$-MET/pure $Zn(ClO_4)_2$ electrolyte.

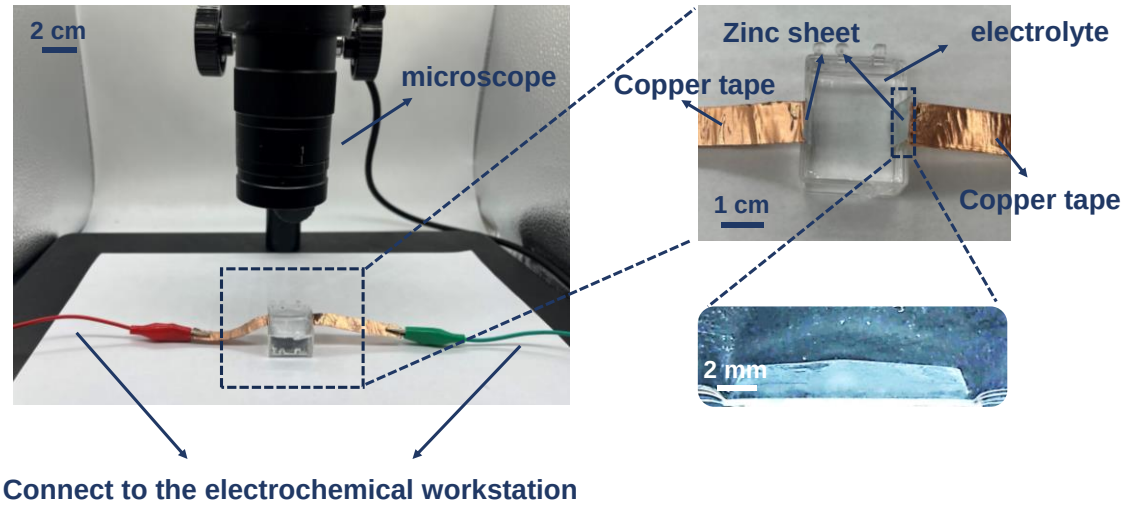

Fig. S8 Optical pictures of the homemade in-situ optical micrograph system and the detailed device image of the in-situ optical micrographs.

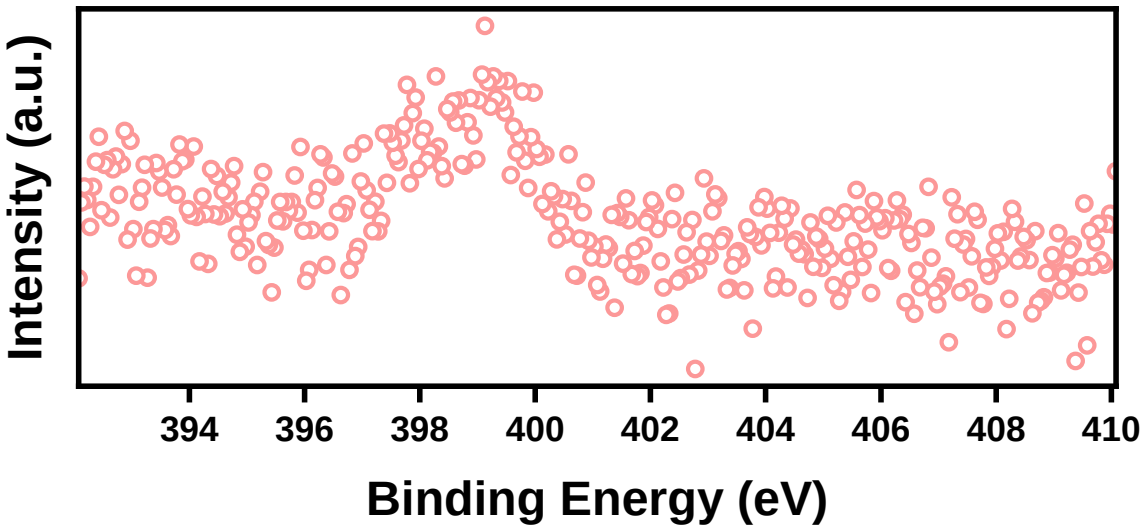

Fig. S9 XPS spectrum of core level N for pure Zn foil.

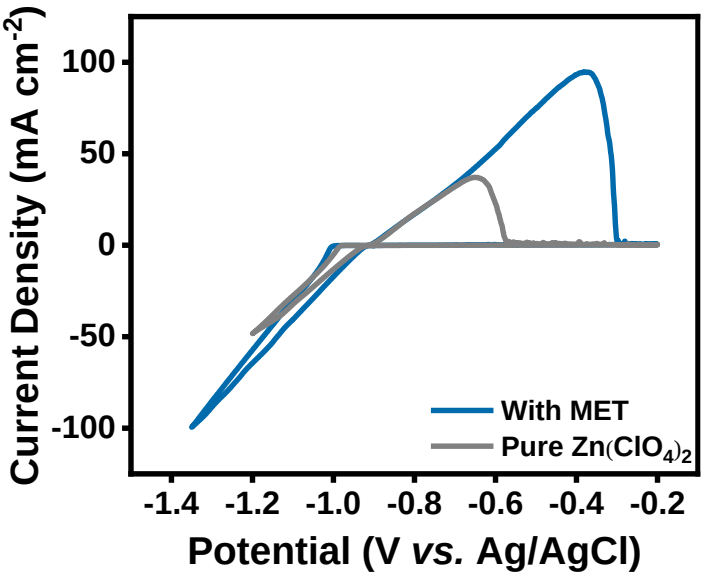

Fig. S10 Cyclic voltammetry curves of Zn plating/stripping processes of different electrolytes in three-electrode systems.

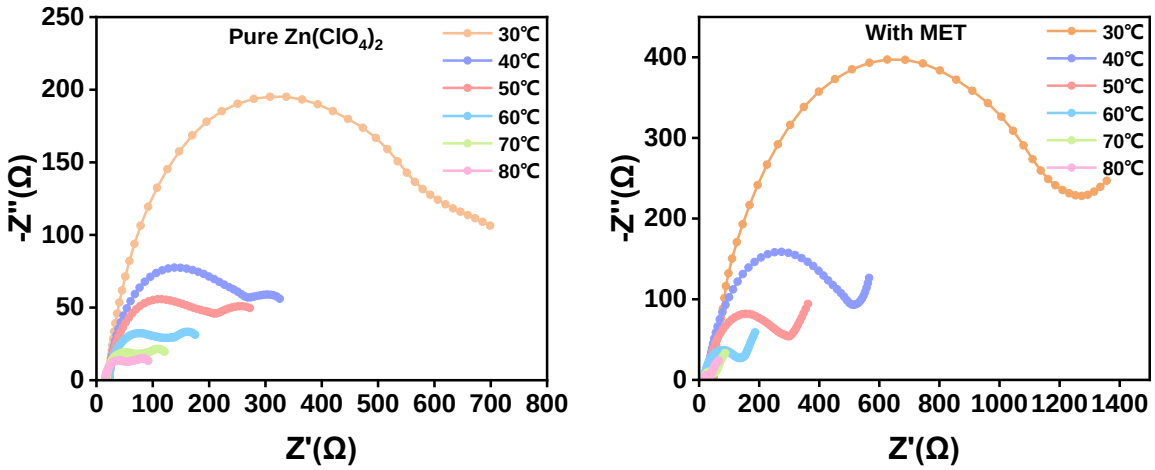

Fig. S11 Nyquist plots of the symmetric cell of different electrolyte systems at different temperatures.

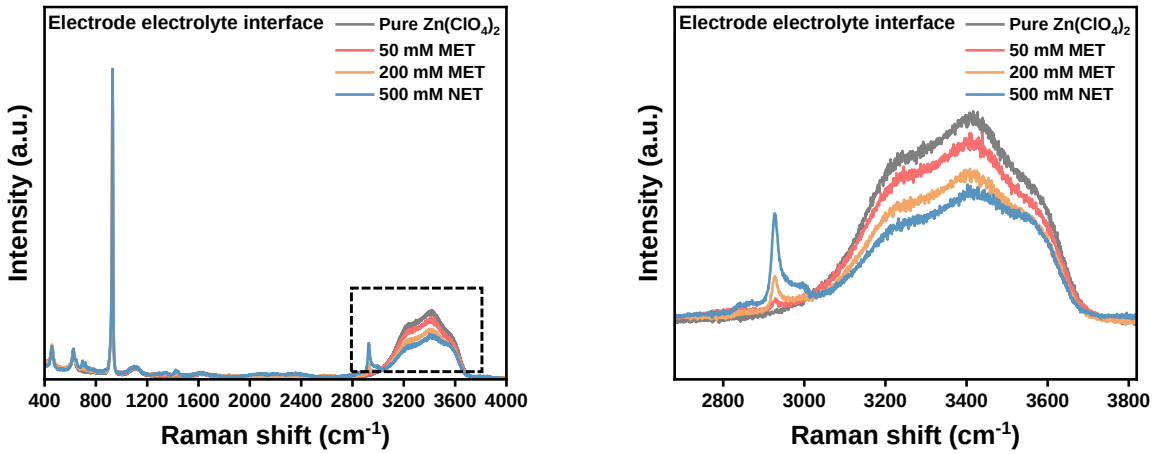

Fig. S12 Raman spectra of the electrode electrolyte interface (EEI) in pure $Zn(ClO_4)_2$ electrolyte system with different MET concentrations.

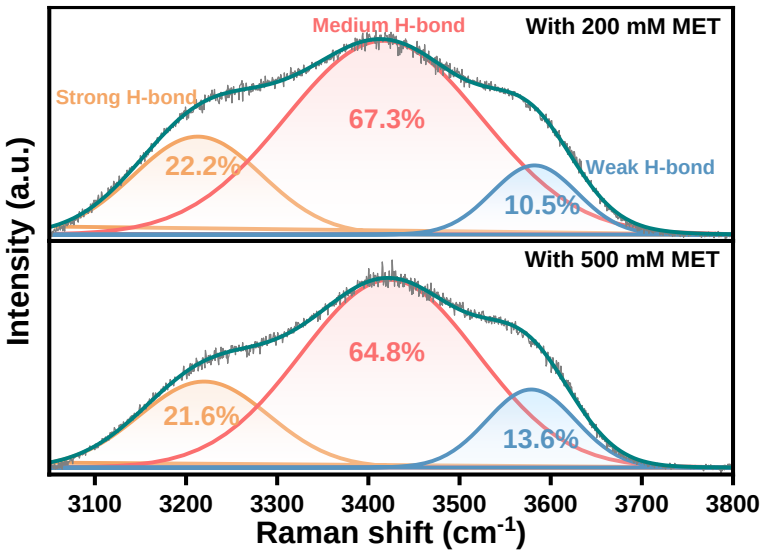

Fig. S13 Raman spectra (3050 cm^{-1} – 3800 cm^{-1}) of EEI in $Zn(ClO_4)_2$-MET electrolyte system with the MET concentrations of 200 mM and 500 mM.

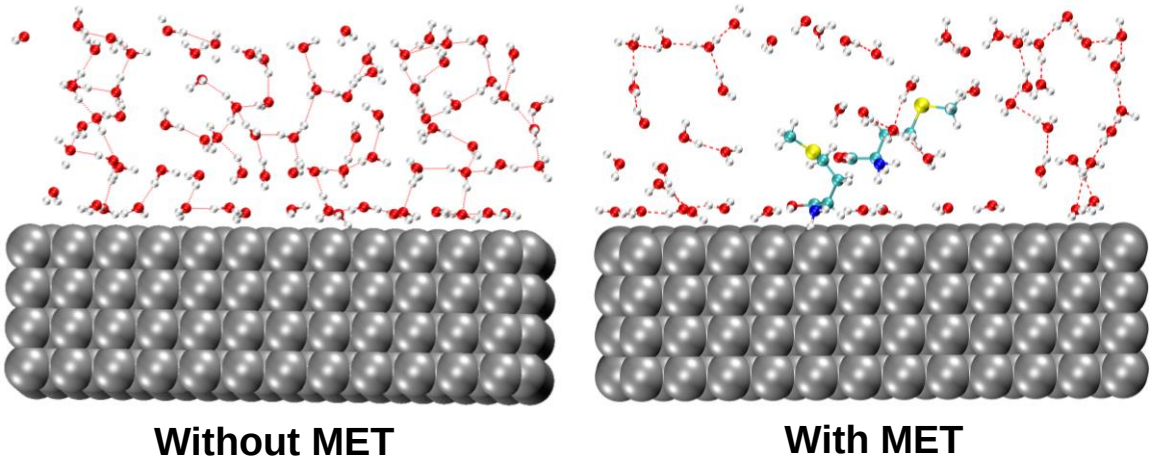

Fig. S14 MD of HB networks at EEI in different electrolyte systems.

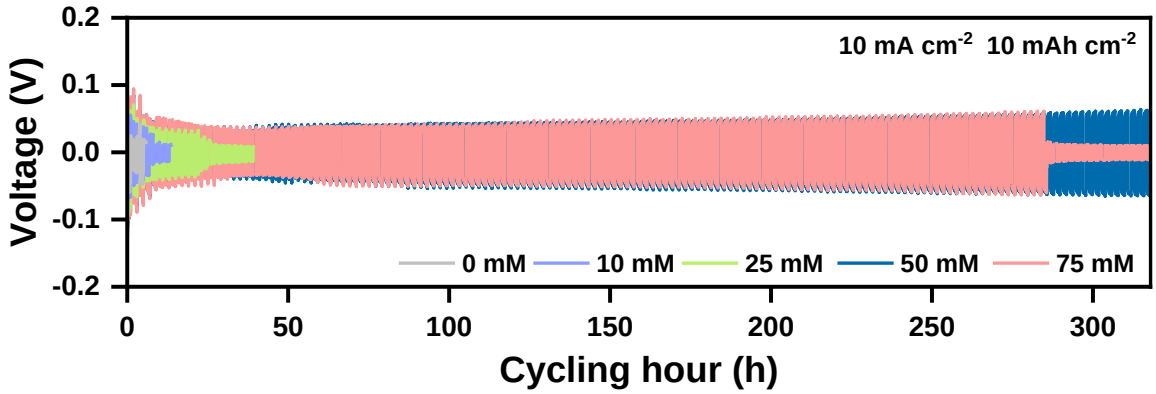

Fig. S15 Long-term cycling performance comparison of Zn//Zn symmetric cells with different MET concentrations under the testing condition of 10 mA cm^{-2}/10 mAh cm^{-2}.

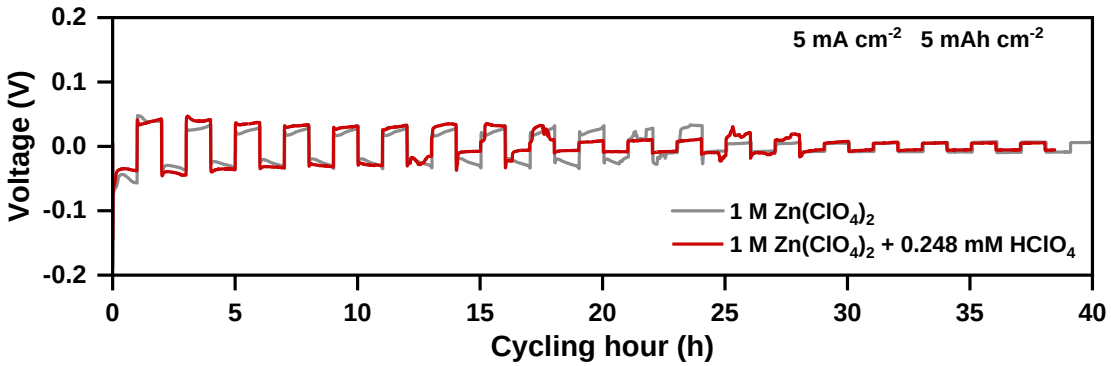

Fig. S16 Long-term cycling performance comparison of Zn//Zn symmetric cells under 5 mA cm^{-2}/5 mAh cm^{-2} in different electrolytes.

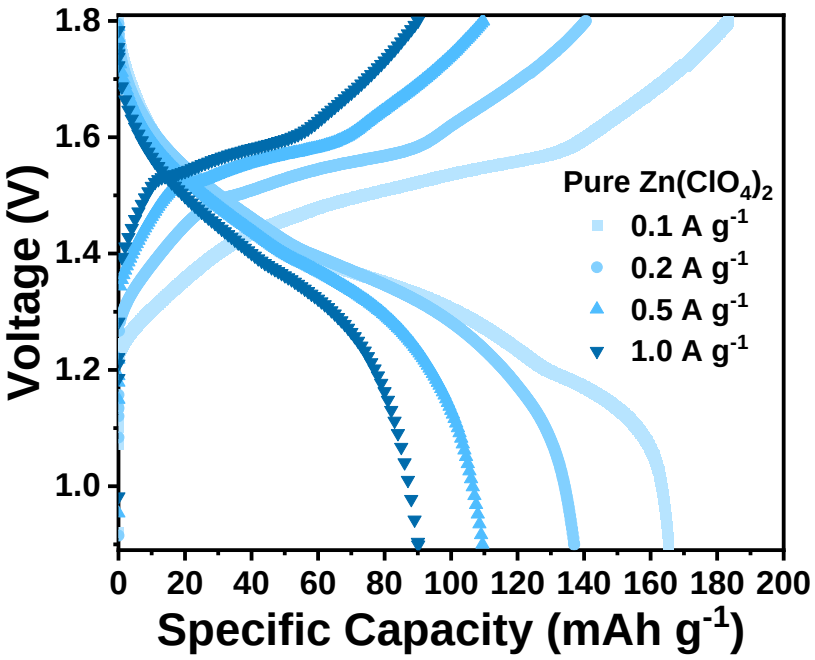

Fig. S17 Corresponding charge–discharge curves of Zn-MnO_2 full cells with the pure $Zn(ClO_4)_2$ electrolyte.

Table S1. Different electrolytes and their pH values.

Electrolyte	pH
1 M $Zn(ClO_4)_2$	3.90
1 M $Zn(ClO_4)_2$ + 50 mM MET	2.93
1 M $Zn(ClO_4)_2$ + 0.248 mM $HClO_4$	2.95

Table S2 Key parameters of recently published aqueous Zn//Zn symmetric cells containing different additives

Electrolyte composition	Current Density (mA cm^{-2})	Per-cycling capacity (mAh cm^{-2})	Cumulative capacity (Ah cm^{-2})	Ref.
$ZnSO_4$ + monosodium glutamate	2 5 10	2 5 10	4.40 8.50 4.30	7
$ZnSO_4$ + histidine	2 5 10	2 2 4	6.00 4.60 2.68	8
$ZnSO_4$ + glycine	1	1	3.20	9
$ZnSO_4$ + benzyl trimethylammonium chloride	1 2 5 10	2 2 5 10	2.00 1.80 2.50 2.25	10
$ZnSO_4$ + bifunctional cholinium	1 2	1 2	2.00 1.60	11
$ZnSO_4$ + CH_3COONH_4	1 4	1 1	2.40 1.60	12
$Zn(CF_3SO_3)_2$ + α-cyclodextrin	1	1	0.50	13
$ZnSO_4$ + glycine	4	2	1.20	14
This work	1 5 10	1 5 10	4.50 5.85 3.18	

Reference

1. J. Hutter, M. Iannuzzi, F. Schiffmann and J. VandeVondele, cp2k: atomistic simulations of condensed matter systems, *Wires. Comput. Mol. Sci.*, 2014, **4**, 15-25.
2. J. VandeVondele, M. Krack, F. Mohamed, M. Parrinello, T. Chassaing and J. Hutter, Quickstep: Fast and accurate density functional calculations using a mixed Gaussian and plane waves approach, *Comput. Phys. Commun.*, 2005, **167**, 103-128.
3. M. T. S. Goedecker, J. Hutter, Separable dual-space Gaussian pseudopotentials, *Phys. Rev. B*, 1996, **54**, 1703-1710.
4. S. G. C. Hartwigsen, J. Hutter, Relativistic separable dual-space Gaussian pseudopotentials from H to Rn, *Phys. Rev. B*, 1998, **58**, 3641-3662.
5. C. K. B. Hess, D. van der Spoel, E. Lindahl, GROMACS 4: Algorithms for Highly Efficient, Load-Balanced, and Scalable Molecular Simulation, *J. Chem. Theory. Comput.*, 2008, **4**, 435-447.
6. E. Lindahl, B. Hess and D. van der Spoel, GROMACS 3.0: a package for molecular simulation and trajectory analysis, *Journal of Molecular Modeling*, 2001, **7**, 306-317.
7. Y. Zhong, Z. Cheng, H. Zhang, J. Li, D. Liu, Y. Liao, J. Meng, Y. Shen and Y. Huang, Monosodium glutamate, an effective electrolyte additive to enhance cycling performance of Zn anode in aqueous battery, *Nano Energy*, 2022, **98**, 107220.
8. Z. Zhao, P. Li, Z. Zhang, H. Zhang and G. Li, Dendrite-free zinc anode enabled by Buffer-like additive via strong cationic specific absorption, *Chem. Eng. J.*, 2023, **454**, 140435.
9. Y. Liu, Y. An, L. Wu, J. Sun, F. Xiong, H. Tang, S. Chen, Y. Guo, L. Zhang, Q. An and L. Mai, Interfacial Chemistry Modulation via Amphoteric Glycine for a Highly Reversible Zinc Anode, *ACS Nano*, 2022, **17**, 552-560.
10. K. Guan, L. Tao, R. Yang, H. Zhang, N. Wang, H. Wan, J. Cui, J. Zhang, H. Wang and H. Wang, Anti-Corrosion for Reversible Zinc Anode via a Hydrophobic Interface in Aqueous Zinc Batteries, *Adv. Energy Mater.*, 2022, **12**, 2103557.
11. X. Nie, L. Miao, W. Yuan, G. Ma, S. Di, Y. Wang, S. Shen and N. Zhang, Cholinium Cations Enable Highly Compact and Dendrite-Free Zn Metal Anodes in Aqueous Electrolytes, *Adv. Funct. Mater.*,

2022, **32**, 2203905.

12. C. Lin, X. Yang, P. Xiong, H. Lin, L. He, Q. Yao, M. Wei, Q. Qian, Q. Chen and L. Zeng, High-Rate, Large Capacity, and Long Life Dendrite-Free Zn Metal Anode Enabled by Trifunctional Electrolyte Additive with a Wide Temperature Range, *Adv. Sci.*, 2022, **9**, e2201433.
13. K. Zhao, G. Fan, J. Liu, F. Liu, J. Li, X. Zhou, Y. Ni, M. Yu, Y. M. Zhang, H. Su, Q. Liu and F. Cheng, Boosting the Kinetics and Stability of Zn Anodes in Aqueous Electrolytes with Supramolecular Cyclodextrin Additives, *J. Am. Chem. Soc.*, 2022, **144**, 11129-11137.
14. Q. Gou, H. Luo, Q. Zhang, J. Deng, R. Zhao, O. Odunmbaku, L. Wang, L. Li, Y. Zheng, J. Li, D. Chao and M. Li, Electrolyte Regulation of Bio-Inspired Zincophilic Additive toward High-Performance Dendrite-Free Aqueous Zinc-Ion Batteries, *Small*, 2023, **19**, e2207502.